International Journal of Applied Earth Observation and Geoinformation 34 (2015) 226–234

Contents lists available at ScienceDirect

International Journal of Applied Earth Observation and Geoinformation

journal homepage: www.elsevier.com/locate/jag

A new approach for surface water change detection: Integration of pixel level image fusion and image classification techniques

Komeil Rokni [a,*], Anuar Ahmad [a], Karim Solaimani [b], Sharifeh Hazini [c]

[a] Department of Geoinformation, Faculty of Geoinformation and Real Estate, Universiti Teknologi Malaysia, 81310 UTM Skudai, Johor, Malaysia
[b] Remote Sensing and GIS Centre, Sari University of Agricultural Sciences and Natural Resources, Sari, Iran
[c] Institute of Geospatial Science & Technology (INSTeG), Universiti Teknologi Malaysia, 81310 UTM Skudai, Johor, Malaysia

ARTICLE INFO

Article history:
Received 6 April 2014
Accepted 19 August 2014
Available online 7 September 2014

Keywords:
Surface water
Change detection
Image fusion
Classification

ABSTRACT

Normally, to detect surface water changes, water features are extracted individually using multi-temporal satellite data, and then analyzed and compared to detect their changes. This study introduced a new approach for surface water change detection, which is based on integration of pixel level image fusion and image classification techniques. The proposed approach has the advantages of producing a pansharpened multispectral image, simultaneously highlighting the changed areas, as well as providing a high accuracy result. In doing so, various fusion techniques including Modified IHS, High Pass Filter, Gram Schmidt, and Wavelet-PC were investigated to merge the multi-temporal Landsat ETM+ 2000 and TM 2010 images to highlight the changes. The suitability of the resulting fused images for change detection was evaluated using edge detection, visual interpretation, and quantitative analysis methods. Subsequently, artificial neural network (ANN), support vector machine (SVM), and maximum likelihood (ML) classification techniques were applied to extract and map the highlighted changes. Furthermore, the applicability of the proposed approach for surface water change detection was evaluated in comparison with some common change detection methods including image differencing, principal components analysis, and post classification comparison. The results indicate that Lake Urmia lost about one third of its surface area in the period 2000–2010. The results illustrate the effectiveness of the proposed approach, especially Gram Schmidt-ANN and Gram Schmidt-SVM for surface water change detection.

Introduction

Surface water is one of the irreplaceable strategic resources for human survival and social development (Ridd and Liu, 1998). It is essential for humans, food crops, and ecosystems (Lu et al., 2011). Reliable information about the spatial distribution of open surface water is critically important in various scientific disciplines, such as the assessment of present and future water resources, climate models, agriculture suitability, river dynamics, wetland inventory, watershed analysis, surface water survey and management, flood mapping, and environmental monitoring (Desmet and Govers, 1996; Zhou and Wu, 2008; Du et al., 2012; Sun et al., 2012). Remote sensing satellites at different spatial, spectral, and temporal resolutions provide an enormous amount of data that have become primary sources, being extensively used for detecting and extracting surface water and its changes in recent decades (Huiping et al., 2011; Senthilnath et al., 2012; Tang et al., 2013; Xu, 2006; Zhang et al., 2003, 2009).

Several image processing techniques have been introduced in recent decades for the extraction of water features from satellite data, such as single-band, multi-band, and classification techniques. Regarding surface water change detection, a review of previous studies indicated that water features are usually extracted individually using multi-temporal satellite data and are then analyzed and compared to detect changes (Alesheikh et al., 2007; Du et al., 2012; El-Asmar and Hereher, 2011; Huiping et al., 2011; López-Caloca et al., 2008; Xu et al., 2010; Zhang et al., 2009). In this study, a new approach based on pixel level fusion of multi-temporal satellite images is introduced for detection of surface water changes. Pixel level image fusion, also known as Pansharpening, is defined as the process of merging different images of a scene on a pixel-by-pixel basis to form a new single composite image more informative than any of the input data (Pohl and Van Genderen, 1998). Various pixel-based image fusion techniques

* Corresponding author. Tel.: +98 911 114 8640.
E-mail addresses: k.rokni@yahoo.com (K. Rokni), anuarahmad@utm.my (A. Ahmad), solaimani2001@yahoo.co.uk (K. Solaimani), sh.hazini@yahoo.com (S. Hazini).

http://dx.doi.org/10.1016/j.jag.2014.08.014
0303-2434/

have been developed, such as Brovey (Gillespie et al., 1987), Intensity-Hue-Saturation (IHS) (Carper et al., 1990), Wavelet transform (Yocky, 1995), Pansharp (Zhang, 2002a,b), Smoothing Filter (Liu, 2000), High Pass Filter (Schowengerdt, 1980), and Local Mean Matching (de Béthune et al., 1998).

In using pixel level image fusion for change detection, usually fusion techniques are applied to sharpen a low resolution multispectral image using a higher resolution panchromatic data to generate enhanced input data for change detection (Bovolo et al., 2010; Du et al., 2013; Gungor and Akar, 2010; Gungor et al., 2010; Lu et al., 2008; Shah and Quackenbush, 2007). Although, in a few studies pixel level fusion of multi-temporal satellite images were used in land/urban areas, this method was found not useful for urban change detection (Du et al., 2013; Zeng et al., 2010). Nevertheless, in this study we explored high performance of multi-temporal pixel level image fusion integrated with advanced image classification techniques for surface water change detection. Since the difference between the reflectance of water and land/dry areas is very high, especially in infrared bands, pixel level fusion of multi-temporal water and dry pixels (the pixels/areas which changed from water in 2000 to dry in 2010) generate new pixels different than other unchanged water and dry pixels. These visible pixels in the fused image are considered as changed areas and can be extracted using image classification techniques. However, the accuracy of change detection result is depending on the image classification technique which applied for the extraction of the changes, as well as the pixel level image fusion technique which applied for the fusion of multi-temporal images to highlight the changes.

Materials and methods

In order to achieve the aims of the study, the following tasks were performed: study area definition, data collection, image pre-processing, image fusion, image quality assessment, image classification, change detection, and accuracy assessment. Fig. 1 shows the overall methods adopted in this study to detect the lake surface area changes.

Study area

Lake Urmia (Urumiyeh in Persian), bound by 37°03′ N to 38°17′ N and 44°59′ E to 45°59′ E, has a maximum depth of 16 m and is about 140 km long and 40–55 km wide (Delju et al., 2012). The lake is a shallow and saline lake that is located in the northwest of Iran (Rokni et al., 2014) (Fig. 2). Lake Urmia has a total catchment area of approximately 51,876 km^2 that is about 3.2% of the size of Iran, and it represents about 7% of the country's surface water (Eimanifar and Mohebbi, 2007). The maximum surface area of the lake has been estimated to be about 6100 km^2, but since 1995, it has been constantly declining and reached 2366 km^2 in August of 2011 (Sima et al., 2013). About 60 rivers (permanent and episodic) are found in the catchment area of the lake all of which flow through agricultural, industrial and urban areas normally without waste water treatment (Eimanifar and Mohebbi, 2007; Ghaheri et al., 1999). The climate of the lake basin is characterized by cold winters and relatively temperate summers, being influenced by the mountains surrounding the lake (Ghaheri et al., 1999). The mean annual

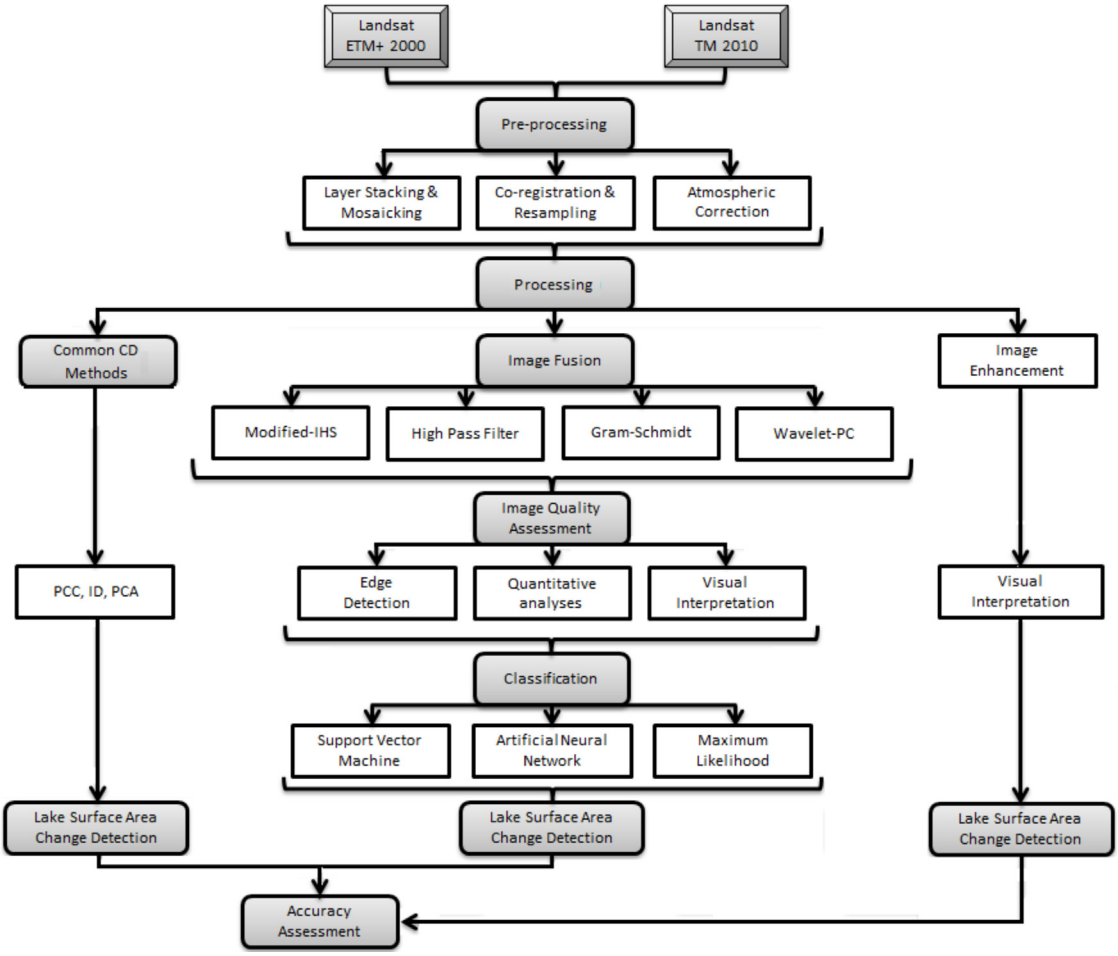

Fig. 1. Flowchart showing the overall methods adopted in this study.

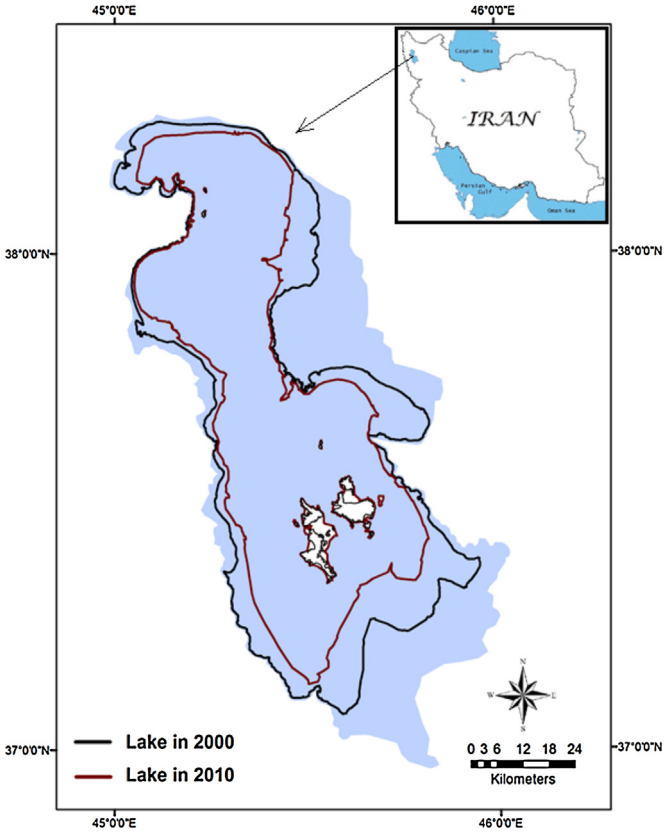

Fig. 2. Location of the study area (Lake Urmia).

precipitation in the catchment area is about 350 mm, and the mean annual evaporation is about 900–1170 mm (Sima et al., 2013).

Data set

Three scenes of Landsat-7 ETM+ data acquired in August 2000 and three scenes of Landsat-5 TM data acquired in July 2010 were obtained from the US Geological Survey (USGS) Global Visualization Viewer. The obtained Landsat data (Level 1 Terrain Corrected (L1T) product) were pre-georeferenced to UTM zone 38 North projection using WGS-84 datum. The other necessary corrections were performed in this study.

Image pre-processing

To prepare the input satellite images for further processing, the following pre-processing steps were performed: radiometric calibration, atmospheric correction, mosaicking, co-registration, and resampling. Radiometric calibration and atmospheric correction were conducted according to (Schroeder et al., 2006). In doing so, the obtained images were converted to at-satellite radiance using the Landsat calibration tool in ENVI 4.8. After conversion to at-satellite radiance, each image was converted to at-satellite reflectance. The required information including the Data Acquisition Date and Sun Elevation was obtained from the Landsat header files. At last, the dark object subtraction (DOS) method (Chavez, 1996), was employed to convert at-satellite reflectance to surface reflectance for full absolute correction.

Subsequently, the images of each year were mosaicked to generate new images covering the entire study area. For this purpose, the mosaicking tool based on georeferenced images was used. For co-registration of the multi-temporal images, one of the images was used as the reference to register the other images. The input images were co-registered with a root mean square error (RMSE) of less than 0.5 pixels using the manual image to image co-registration method. Finally, the dataset were resampled to the same size of the study area using the Nearest Neighbor method.

Surface water change detection using the integrated image fusion-image classification approach

The proposed approach is consisting of three steps: (i) pixel level fusion of multi-temporal Landsat ETM+ Pan (15 m) 2000 and Landsat TM multispectral (30 m) 2010 images to obtain a sharpened image which highlighted the changed areas, (ii) image quality assessment, which is performed to evaluate suitability of the fused images for highlighting the changed areas, and (iii) image classification, which is applied to extract and map the highlighted change areas/pixels.

Multi-temporal image fusion

Image fusion at pixel level requires a higher resolution panchromatic band and a lower resolution multispectral image to be executed. In this study, four popular pixel level image fusion techniques including Modified IHS (Intensity, Hue, Saturation) (Siddiqui, 2003), High Pass Filter (HPF) (Schowengerdt, 1980), Gram Schmidt (GS) (Laben et al., 2000), and Wavelet-PC (Principal Components) (Yocky, 1995) were examined to merge the multi-temporal Landsat ETM+ 2000 band 8 (15 m) and Landsat TM 2010 multispectral (30 m) images to obtain a sharpened image as well as highlighting the changed areas between the two times.

To merge the input images using Modified IHS algorithm, three bands of the multispectral image are transformed from the RGB domain to the IHS color space. Next, the panchromatic band is matched to the intensity component of the IHS color space and then replaced with this component. Last step is transforming back to the RGB color space. The output result is the fused image (Klonus and Ehlers, 2007). Modified IHS was developed by Siddiqui (2003) for better fitting between the bands of fused and original images.

To perform High Pass Filter algorithm, first the ratio between the multispectral cell size to the panchromatic cell size is calculated. High Pass Filter of the panchromatic band is then derived. This operation produces the High Pass Filter image. A high pass convolution filter kernel (HPK) is generated and used to filter the panchromatic data. The size of HPK is a function of the relative input pixel sizes. All values of the kernel are set to −1 except the center value. Subsequently, the multispectral image is resampled to the pixel size of the high pass image. The HPF image is then added to each band of the multispectral data. Finally, the new multispectral image is stretched to match the mean and standard deviation of the original multispectral image. The output result is the fused image (Aiazzi et al., 2002; Klonus and Ehlers, 2009).

To merge the input dataset using Gram Schmidt algorithm, a panchromatic band is simulated from the multispectral bands. It is obtained by averaging the bands of multispectral image. A Gram Schmidt transformation is then executed to the simulated panchromatic and multispectral bands. Next, the panchromatic band is replaced with the first GS band. Finally, an inverse Gram Schmidt transformation is applied to form the fused image (Klonus and Ehlers, 2007; Laben et al., 2000).

To perform Wavelet-PC algorithm, first, the multispectral bands are converted to a new set of uncorrelated Principal Components (PCs). Next, histogram matching between the panchromatic image and the PC1 is performed and a new panchromatic image is acquired. The PC1 and new panchromatic image are then decomposed to detailed coefficients and approximate coefficients for each level. Subsequently, the high detailed coefficients of PC1 are

replaced with those of the new panchromatic band, and the new wavelet coefficients of PC1 are transformed to obtain a new PC1. At last, an inverse transformation is performed to obtain the fused image (Rokni et al., 2011).

Image quality assessment

The quality of the resulting fused images was assessed using the visual and quantitative analyses methods. In this study, we were looking for the fused image which properly highlighted the changed areas. In this respect, the quality assessment methods based on visual analyses including edge detection and visual interpretation were preferred. However, the quantitative analyses were also performed to ensure the spectral fidelity of the fused image.

In doing so, the Laplacian filter as a standard non-directional edge detection filter was applied to the fused images. The edges to be detected were the coastlines of the lake in the years 2000 and 2010. In addition, visual interpretation was carried out to support the results of edge detection. Visual interpretation was implemented by cropping some sample subsets from the fused images and visually inspecting for any changes between the two times. Finally, various statistical criteria/metrics were used to assess quality of the fused image (Table 1).

Image classification

In last step, the artificial neural network (ANN), support vector machine (SVM), and maximum likelihood (ML) classification techniques were applied to extract and map the surface water changes identified in the fused image.

ANN is a recent non-parametric classification technique that requires no assumptions about the feature's distribution (distribution free) and little or no a priori knowledge about the statistical characteristics of feature class data (Li et al., 2011). Furthermore, ANN can perform well with small training sets and is well resistant to noise or incomplete sampling of spectra in simulated satellite data (Song et al., 2012). The neural network classifier adopted in this study is a non-linear layered feedforward model with standard backpropagation for supervised learning. This category of ANN logistic was preferred because of its facility to learn by pattern (Srivastava et al., 2012). This ANN model consists of three types of layers: input layer, at least one hidden layer, and the output layer. The default values in ENVI software were set to perform ANN in this study.

SVM is a supervised machine learning technique that performs classification based on statistical learning theory and aims to determine the location of decision boundaries that produce the optimal separation of the classes (Pal and Foody, 2012; Petropoulos et al., 2012). In this study, a multiclass SVM pair-wise classification strategy was performed. This technique, like ANN, consists of the input and output layers. Besides, selection of a proper kernel type is an important factor in SVM classification. The Radial Basic Function kernel was used for performing the pair-wise SVM classification in the study. The rationale for selection of this kernel is guided by the fact that it requires definition of a few parameters

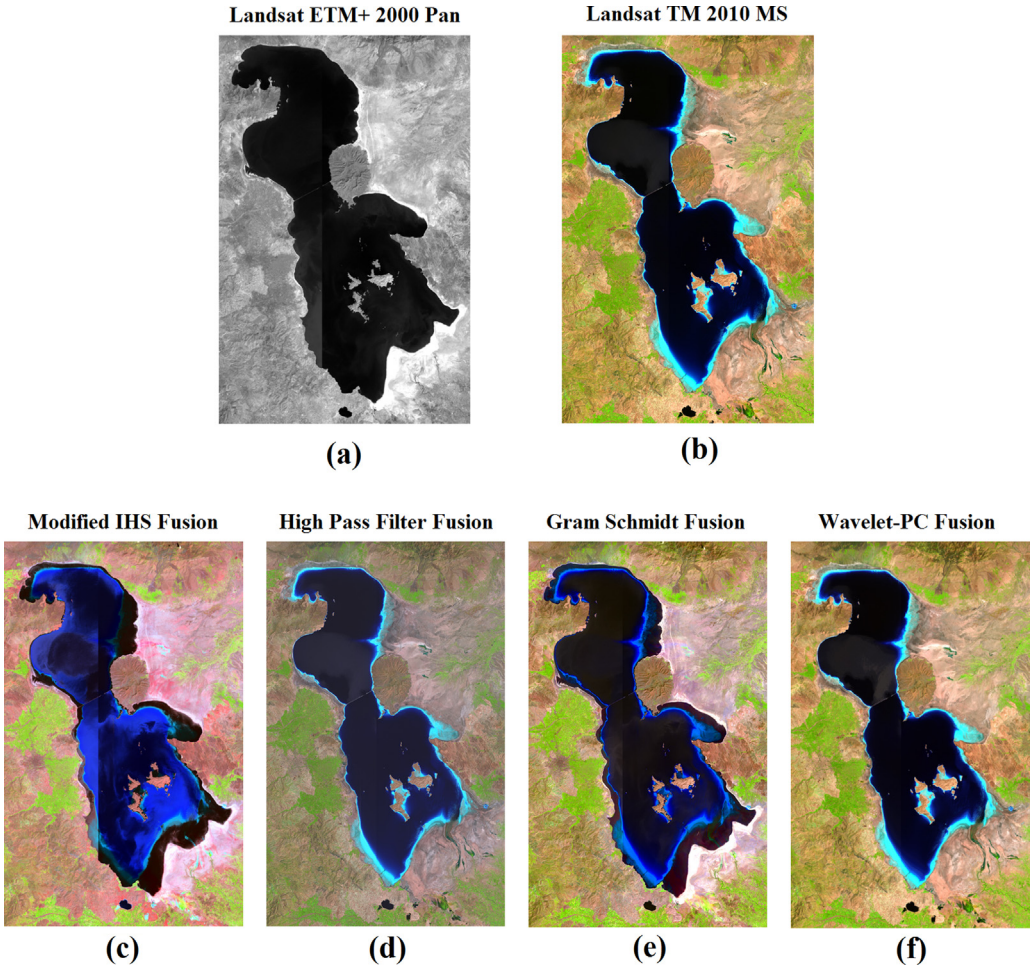

Fig. 3. The original (a) Landsat ETM+ band 8 2000 and (b) Landsat TM multispectral 2010 images, and the fused images using (c) Modified IHS, (d) High Pass Filter, (e) Gram Schmidt, and (f) Wavelet-PC techniques.

Table 1
Statistical criteria used to assess quality of the fused image (where, μ_F is the mean value of the fused image, μ_O = mean value of the original multispectral image, σ_F = standard deviation of the fused image, σ_O = standard deviation of the original multispectral image, and σ_F^2 and σ_O^2 are variances of the fused and original images, respectively).

Criteria	Equation	Remark
Relative mean difference	$RMD = (\mu_F - \mu_O)/\mu_O$	Ideal value is 0
Relative variation difference	$RVD = (\sigma_F^2 - \sigma_O^2)/\sigma_O^2$	Ideal value is 0
Root mean square error	$RMSE = \sqrt{\mu^2 + \sigma^2}$ $\mu = \mu_O - \mu_F$, $\sigma = \sigma_O - \sigma_F$	Ideal value is 0
Contrast similarity	$CS = (2\sigma_O\sigma_F/\sigma_O^2 + \sigma_F^2)$	Ideal value is +1
Correlation coefficient	$CC = \sigma_{OF}/\sigma_O\sigma_F$	Ideal value is +1
Universal image quality index	$UIQI = (\sigma_{OF}/\sigma_O\sigma_F)\cdot(2\mu_O\mu_F/\mu_O^2 + \mu_F^2)\cdot(2\sigma_O\sigma_F/\sigma_O^2 + \sigma_F^2)$	Ideal value is +1

to run, and has also shown to produce generally promising result (Petropoulos et al., 2012). The Gamma in kernel function was set to a value of 0.143 as default in ENVI software. The penalty parameter, which controls the trade-off between allowing training errors and forcing rigid margins, was set in to a value of 100 to create the most accurate possible model. The pyramid parameter was set to zero, meaning that each image should be processed at full resolution. Finally, a classification probability threshold of zero was applied forcing all image pixels to be classified into a class label and have no unclassified pixels in the image.

The results of ANN and SVM to extract surface water changes from the fused image were compared to the ML classifier. ML is the most common parametric classifier that assumes normal or near-normal spectral distribution for each feature of interest and calculates the probability that a given pixel belongs to a specific class. The ML considers both the variance and covariance of the class signatures when assigning each cell to one of the classes represented in the signature file. When a priori option is specified (equal weighting), each cell is classified to the class to which it has the highest probability of being a member. A detailed description about ML is available in many published literature such as (Jensen, 2004; Lillesand et al., 2004).

Surface water change detection using the most common change detection methods

Reviewing the previous studies indicated that post classification comparison (PCC), image differencing (ID), and principal component analysis (PCA) were the most common methods used for different change detection applications. Therefore, the suitability of the proposed image fusion-image classification approach for surface water change detection was evaluated in comparison with these change detection methods.

To perform PCC change detection method, the multi-temporal images were independently classified using the ML technique. The classified images were then analyzed and compared on a pixel-by-pixel basis to detect the changes. The ID method was performed by subtracting the digital number (DN) values of the pixels in one date image from the DN values of the same pixels in another date image. In doing so, the band 4 of multi-temporal Landsat images was selected due to its higher capability to separate dry and water pixels/areas. To perform PCA method, the multi-temporal Landsat images were stacked into a single file. The PCA technique was then applied to the composite image and the resulting principal components (PCs) were analyzed for detecting the changes.

Accuracy assessment

Lack of a reliable ground truth reference is a common problem in accuracy assessment of change detection results. To overcome this limitation, a lake surface area change map was generated using visual interpretation as the reference to assess the accuracy of the achieved change detection results. For visual interpretation of water bodies, the near-infrared (NIR) band is usually preferred, because NIR is strongly absorbed by water and is strongly reflected by terrestrial vegetation and dry soil (Sun et al., 2012). Thus, band 4 of Landsat data was selected due to its higher ability to discriminate between water and dry/land areas. The reference change map was generated utilizing careful on-screen digitizing of the lake surface area in multi-temporal Landsat ETM+ 2000 and TM 2010 images using visual interpretation and overlaying the results in ArcGIS environment. Image enhancement was performed earlier to band 4 of multi-temporal Landsat data to facilitate definition of the land-water interface. The performances of different change detection methods applied in this study were initially evaluated through calculation of Absolute and Relative Errors. Absolute Error is the difference between the changed areas detected using the applied method and the reference, whereas Relative Error corresponds with the percentage of those differences. In addition, overall accuracy and Kappa coefficient were calculated to support the accuracy assessment analyses.

Results and discussion

Image fusion and quality assessment

The results of the fusion techniques applied to merge the multi-temporal Landsat ETM+ panchromatic (2000) and Landsat TM multispectral (2010) images are shown in Fig. 3.

The suitability of the resultant fused images for surface water change detection was first evaluated using the Laplacian edge detection filter (Fig. 4). The edge detection results show that the coastlines of the lake in 2000 and 2010 are well detected in the Gram Schmidt fused image (Fig. 4c). The coastline of the lake in 2000 is not detected in the High Pass Filter and Wavelet-PC fused images (Fig. 4b and d). Although the coastline of the lake in 2000 is very well detected in the Modified IHS fused image, the coastline of the lake in 2010 is not well detected in this image (Fig. 4a). The achieved results indicate superiority of the Gram Schmidt fused image to other fused images in detecting the lake coastlines in 2000 and 2010, consequently detecting the changes between the two times.

Subsequently, the suitability of the resultant fused images for surface water change detection was evaluated using visual interpretation. To simplify visual interpretation, some sample subsets were cropped from the fused images and were inspected visually for any change between the two times (Fig. 5). Similar to edge detection, visual interpretation of the fused images also indicates superiority of the Gram Schmidt fused image to other fused images in highlighting the lake surface area changes (Fig. 5c). The results show that the changed areas are not highlighted in the High Pass Filter and Wavelet-PC fused images (Fig. 5b and d). Although the

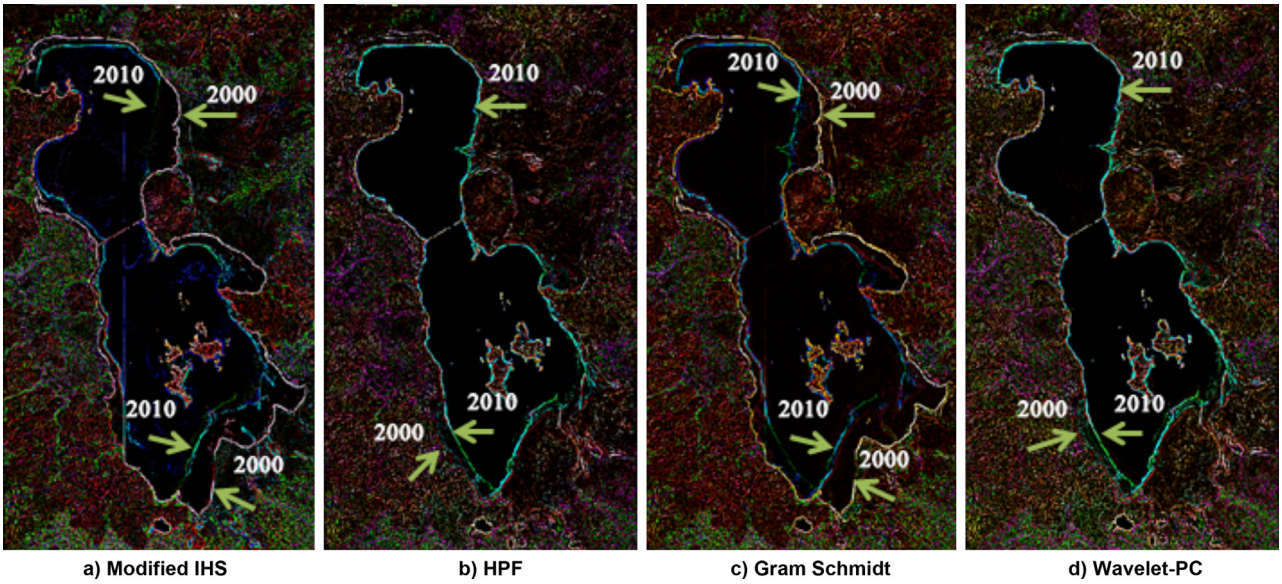

Fig. 4. Laplacian edge detection filter applied to the fused images.

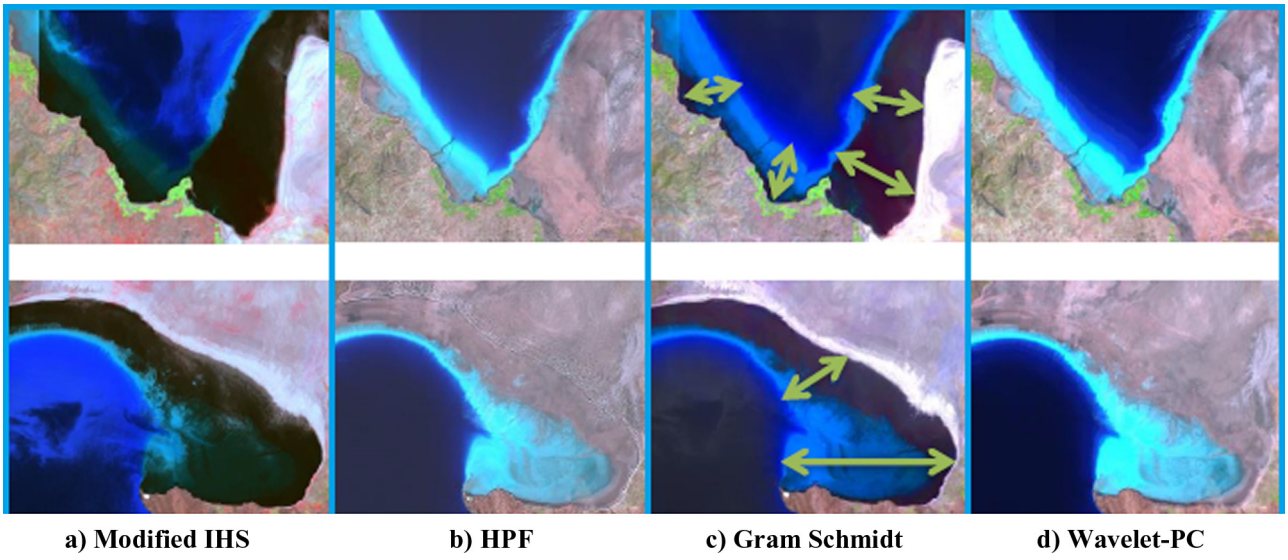

Fig. 5. Visual interpretation of the fused images.

changed areas are highlighted in the Modified IHS fused image, some color distortions are appeared in this image (Fig. 5a). Conversely, the Gram Schmidt fused image very well highlighted the changed areas with less or no distortion.

Based on the results of both edge detection and visual interpretation, the Gram Schmidt fused image was preferred for further processing. Before applying the classification techniques to the Gram Schmidt fused image to extract and map the lake surface area changes, some statistical metrics were used to ensure the spectral fidelity of this fused image. The results, summarized in Table 2, reveal closeness of the achieved values to the ideal values that prove suitability of the Gram Schmidt fused image in preserving the spectral quality.

Surface water change detection and mapping

Once the image fusion and image quality assessment steps were successfully performed, the artificial neural network, support vector machine, and maximum likelihood techniques were applied to the Gram Schmidt fused image to extract and map the lake surface area changes between the years 2000 and 2010. Using the specified classification techniques, the Gram Schmidt fused image was categorized into three classes including water area, changed area, and land area. Water area is the lake surface area in 2010, changed area is the lake surface area that was changed from water in 2000 to land in 2010, and land area is the lake surface area

Table 2
Statistical criteria used to assess quality of the Gram Schmidt fused image.

Criteria	Achieved value	Ideal value
RMD	0.009	0
RVD	0.091	0
RMSE	2.170	0
CS	0.990	1
CC	0.820	1
UIQI	0.800	1

that was dried before 2000. The change detection results achieved using the proposed approach were then compared with the results of post classification comparison, image differencing, and principal components analysis as the most common change detection methods. The lake surface area change maps generated using Gram Schmidt-ANN, Gram Schmidt-SVM, Gram Schmidt-ML, post classification comparison, image differencing, principal components analysis, and visual interpretation methods are shown in Fig. 6.

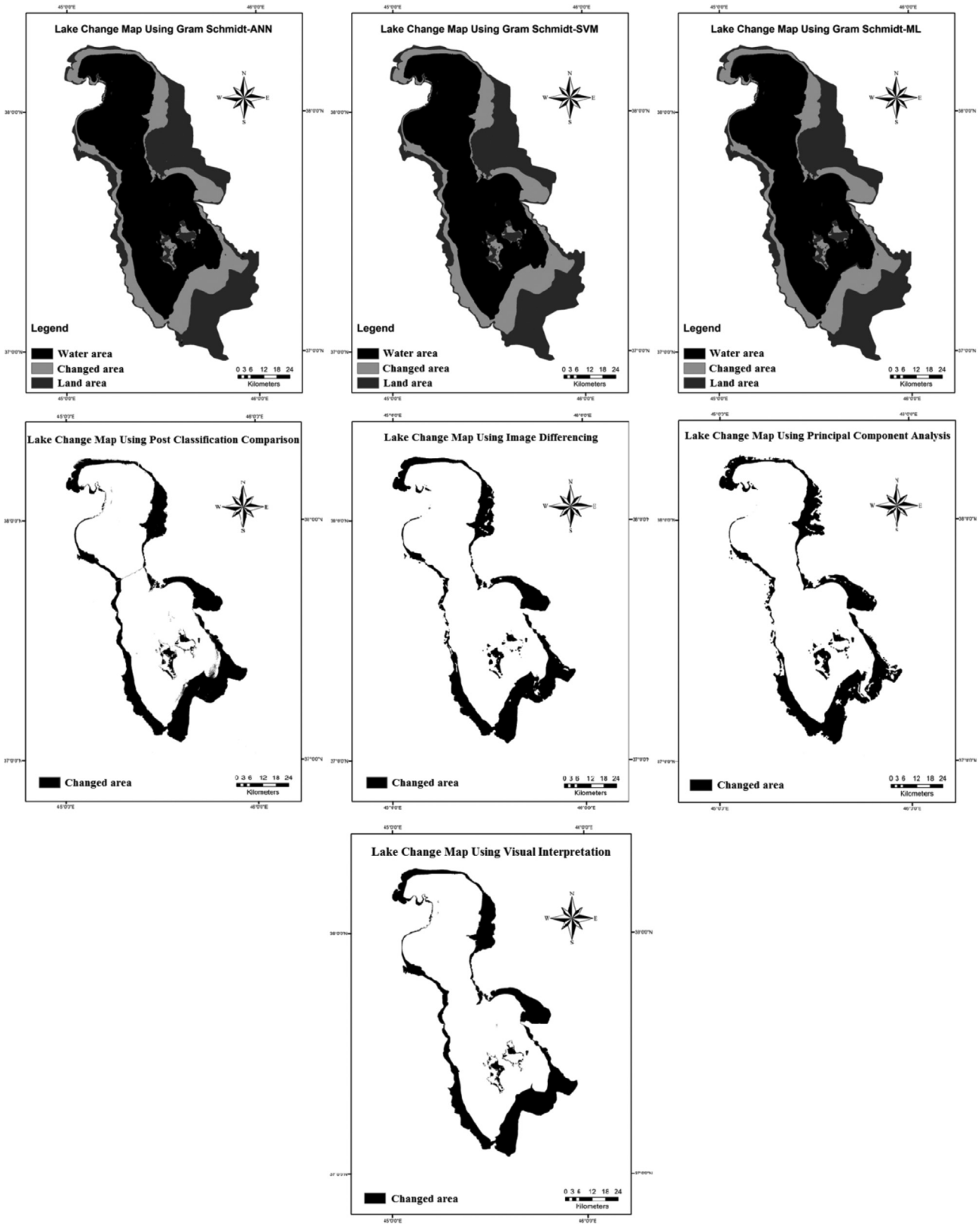

Fig. 6. Lake surface area change maps generated using: (a) Gram Schmidt-ANN, (b) Gram Schmidt-SVM, (c) Gram Schmidt-ML, (d) post classification comparison, (e) image differencing, (f) principal components analysis, and (g) visual interpretation methods.

Table 3
Statistics of the generated change maps.

Method	Lake area in 2000 (km^2)	Lake area in 2010 (km^2)	Lake area change between 2000 and 2010 (km^2)
Visual interpretation	4699	3328	1371
Gram Schmidt-ANN	4694	3327	1367
Gram Schmidt-SVM	4693	3316	1377
Gram Schmidt-ML	4654	3298	1356
Post classification comparison	4621	3231	1390
Image differencing	–	–	1338
Principal component analysis	–	–	1418

The results, summarized in Table 3, indicate that the lake surface area from July 2000 to August 2010 has decreased about 1367 km^2 based on Gram Schmidt-ANN, 1377 km^2 based on Gram Schmidt-SVM, 1356 km^2 based on Gram Schmidt-ML, 1390 km^2 based on post classification comparison, 1338 km^2 based on image differencing, and 1418 km^2 based on principal components analysis methods. Based on the result of visual interpretation as the reference, the lake surface area has shrunk about 1371 km^2 in this period experiencing an approximate 29% shrinkage in 2010 compared to 2000. It means that Lake Urmia lost about one third of its surface area in the period 2000–2010. The maximal changes are observed around the southern and eastern parts of the lake.

Accuracy assessment analyses (Table 4) reveal superiority of the Gram Schmidt-ANN and Gram Schmidt-SVM approaches for surface water change detection compared with other methods. The Gram Schmidt-ANN achieved an Absolute Error of 4 km^2, a Relative Error of 0.29%, an Overall Accuracy of 99.89%, and a Kappa Coefficient of 0.91. The Gram Schmidt-SVM achieved an Absolute Error of 6 km^2, a Relative Error of 0.44%, an Overall Accuracy of 99.87%, and a Kappa Coefficient of 0.91. The Gram Schmidt-ML and post classification comparison methods with the overall accuracies of more than 99% also provided reliable results for surface water change detection, whereas the image differencing and principal component analysis methods could not relatively achieve reasonable results.

The achieved results demonstrate high performance of the proposed approach based on integration of pixel level image fusion and advanced image classification techniques for surface water change detection, especially using the Gram Schmidt-ANN and Gram Schmidt-SVM approaches which provided the highest accuracy outcomes. The ANN and SVM techniques successfully separated the changed areas from the other unchanged water and land areas in the Gram Schmidt fused image and extracted the changes with a high accuracy. The proposed approach has the advantages of performing the Pansharpening to produce a high resolution multispectral image (ETM+ panchromatic 15 m + TM multispectral 30 m = Fused image multispectral 15 m), at the same time highlighting the changed areas in the resulting fused image, as well as providing a reliable result.

Table 4
Accuracy assessment analyses.

Method	Absolute error (km^2)	Relative error (%)	Overall accuracy (%)	Kappa coefficient
Visual interpretation	0	0.00	100	1
Gram Schmidt-ANN	4	0.29	99.89	0.91
Gram Schmidt-SVM	6	0.44	99.87	0.91
Gram Schmidt-ML	15	1.09	99.13	0.89
Post classification comparison	19	1.38	99.37	0.90
Image differencing	33	2.41	98.33	0.88
Principal component analysis	47	3.43	97.67	0.86

Conclusion

The study introduced a new approach based on integration of image fusion and image classification techniques for surface water change detection. The effectiveness of the proposed approach for detecting the lake surface area changes was proven in comparison with some common change detection methods. The results demonstrated high performance of the suggested approach for detection of surface water changes, especially using the Gram-Schmidt-ANN and Gram Schmidt-SVM approaches which provided a very high accuracy results. The proposed approach has the advantages of producing a high resolution multispectral image, simultaneously highlighting the changed areas in the resulting fused image, as well as providing a reliable result. Although, multi-temporal pixel level image fusion was found not useful for urban change detection, this study revealed suitability of this approach integrated with advanced image classification techniques for monitoring surface water changes. In conclusion, the proposed approach has been proven to be effective in detecting the water surface changes of Lake Urmia, Iran. Accordingly, the method may prove useful in studying other surface waters in the world as well as flood monitoring.

Acknowledgments

The authors would like to thank Universiti Teknologi Malaysia (UTM) and Sari University of Agricultural Sciences and Natural Resources for providing the facilities for this investigation. We are also grateful to U.S. Geological Survey (USGS) for providing the multi-temporal Landsat data.

References

Aiazzi, B., Alparone, L., Baronti, S., Garzelli, A., 2002. Context-driven fusion of high spatial and spectral resolution images based on oversampled multiresolution analysis. IEEE Trans. Geosci. Remote Sens. 40, 2300–2312.
Alesheikh, A.A., Ghorbanali, A., Nouri, N., 2007. Coastline change detection using remote sensing. Int. J. Environ. Sci. Technol. 4, 61–66.
Bovolo, F., Bruzzone, L., Capobianco, L., Garzelli, A., Marchesi, S., Nencini, F., 2010. Analysis of the effects of pansharpening in change detection on VHR images. IEEE Geosci. Remote Sens. Lett. 7, 53–57.
Carper, W.J., Lillesand, T.M., Kiefer, R.W., 1990. The use of intensity-hue-saturation transformations for merging SPOT panchromatic and multispectral image data. Photogramm. Eng. Remote Sens. 56, 459–467.
Chavez Jr., P.S., 1996. Image-based atmospheric corrections – revisited and improved. Photogram. Eng. Remote Sens. 62, 1025–1036.
de Béthune, S., Muller, F., Donnay, J.P., 1998. Fusion of multispectral and panchromatic images by local mean and variance matching filtering techniques, Proceedings of the Second International Conference. In: Ranchin, T., Wald, L. (Eds.), Fusion of Earth Data Merging Point Measurements, Raster Maps and Remotely Sensed Images. EARSeL-SEE-Ecole des Mines de, Paris, pp. 31–36, 28-30 January.
Delju, A.H., Ceylan, A., Piguet, E., Rebetez, M., 2012. Observed climate variability and change in Urmia Lake Basin, Iran. Theor. Appl. Climatol. 111, 285–296.
Desmet, P.J.J., Govers, G., 1996. A GIS procedure for automatically calculating the USLE LS factor on topographically complex landscape units. J. Soil Water Conserv. 51, 427–433.
Du, Z., Linghu, B., Ling, F., Li, W., Tian, W., Wang, H., Gui, Y., Sun, B., Zhang, X., 2012. Estimating surface water area changes using time-series Landsat data in the Qingjiang River Basin, China. J. Appl. Remote Sens. 6, 063609.
Du, P., Liu, S., Xia, J., Zhao, Y., 2013. Information fusion techniques for change detection from multi-temporal remote sensing images. Inf. Fusion 14, 19–27.
Eimanifar, A., Mohebbi, F., 2007. Urmia Lake (Northwest Iran): a brief review. Saline Syst. 3, 1–8.
El-Asmar, H.M., Hereher, M.E., 2011. Change detection of the coastal zone east of the Nile Delta using remote sensing. Environ. Earth Sci. 62, 769–777.
Ghaheri, M., Baghal-Vayjooee, M., Naziri, J., 1999. Lake Urmia, Iran: a summary review. Int. J. Salt Lake Res. 8, 19–22.
Gillespie, A.R., Kahle, A.B., Walker, R.E., 1987. Color enhancement of highly correlated images. II. Channel ratio and "chromaticity" transformation techniques. Remote Sens. Environ. 22, 343–365.
Gungor, O., Akar, O., 2010. Multi sensor data fusion for change detection. Sci. Res. Essays 5, 2823–2831.
Gungor, O., Boz, Y., Gokalp, E., Comert, C., Akar, A., 2010. Fusion of low and high resolution satellite images to monitor changes on costal zones. Sci. Res. Essays 5, 654–662.

Huiping, Z., Hong, J., Qinghua, H., 2011. Landscape and water quality change detection in urban wetland: a post-classification comparison method with IKONOS data. Procedia Environ. Sci. 10, 1726–1731.
Jensen, J.R., 2004. Introductory Digital Image Processing: A Remote Sensing Perspective. Pearson Prentice Hall, Upper Saddle River, NJ.
Klonus, S., Ehlers, M., 2007. Image fusion using the Ehlers spectral characteristics preservation algorithm. GISci. Remote Sens. 44, 93–116.
Klonus, S., Ehlers, M., 2009. Performance of evaluation methods in image fusion. In: 12th International Conference on Information Fusion Seattle, WA, USA, pp. 1409–1416.
Laben, C.A., Bernard, V., Brower, W., 2000. Process for enhancing the spatial resolution of multispectral imagery using pan-sharpening. U.S. Patents 6,011,875.
Li, G., Lu, D., Moran, E., Hetrick, S., 2011. Land-cover classification in a moist tropical region of Brazil with Landsat Thematic Mapper imagery. Int. J. Remote Sens. 32, 8207–8230.
Lillesand, T.M., Kiefer, R.W., Chipman, J.W., 2004. Remote Sensing and Image Interpretation. John Wiley & Sons Ltd.
Liu, J., 2000. Smoothing filter-based intensity modulation: a spectral preserve image fusion technique for improving spatial details. Int. J. Remote Sens. 21, 3461–3472.
López-Caloca, A., Tapia-Silva, F.-O., Escalante-Ramírez, B., 2008. Lake Chapala change detection using time series. Remote Sens. Agric. Ecosyst. Hydrol. 7104, 1–11.
Lu, D., Batistella, M., Moran, E., 2008. Integration of landsat TM and SPOT HRG images for vegetation change detection in the Brazilian amazon. Photogram. Eng. Remote Sens. 74, 421–430.
Lu, S., Wu, B., Yan, N., Wang, H., 2011. Water body mapping method with HJ-1A/B satellite imagery. Int. J. Appl. Earth Obs. Geoinf. 13, 428–434.
Pal, M., Foody, G.M., 2012. Evaluation of SVM, RVM and SMLR for accurate image classification with limited ground data. IEEE J. Sel. Top. Appl. Earth Obs. Remote Sens. 5, 1344–1355.
Petropoulos, G.P., Kontoes, C.C., Keramitsoglou, I., 2012. Land cover mapping with emphasis to burnt area delineation using co-orbital ALI and Landsat TM imagery. Int. J. Appl. Earth Obs. Geoinf. 18, 344–355.
Pohl, C., Van Genderen, J., 1998. Review article Multisensor image fusion in remote sensing: concepts, methods and applications. Int. J. Remote Sens. 19, 823–854.
Ridd, M.K., Liu, J., 1998. A comparison of four algorithms for change detection in an urban environment. Remote Sens. Environ. 63, 95–100.
Rokni, K., Hashim, M., Hazini, S., 2011. Fusion of aster and radarsat sar data using different transforming algorithms of wavelet resolution merge. Aust. J. Basic Appl. Sci. 5, 991–998.
Rokni, K., Ahmad, A., Selamat, A., Hazini, S., 2014. Water feature extraction and change detection using multitemporal Landsat imagery. Remote Sens. 6, 4173–4189.
Schowengerdt, R.A., 1980. Reconstruction of multispatial, multispectral image data using spatial frequency content. Photogramm. Eng. Remote Sens. 46, 1325–1334.
Schroeder, T.A., Cohen, W.B., Song, C., Canty, M.J., Yang, Z., 2006. Radiometric correction of multi-temporal Landsat data for characterization of early successional forest patterns in western Oregon. Remote Sens. Environ. 103, 16–26.
Senthilnath, J., Bajpai, S., Omkar, S.N., Diwakar, P.G., Mani, V., 2012. An approach to multi-temporal MODIS image analysis using image classification and segmentation. Adv. Space Res. 50, 1274–1287.
Shah, C.A., Quackenbush, L.J., 2007. Analyzing multi-sensor data fusion techniques: a multi-temporal change detection approach. In: American Society for Photogrammetry and Remote Sensing: Identifying Geospatial Solutions, pp. 656–665.
Siddiqui, Y., 2003. The modified IHS method for fusing satellite imagery. In: ASPRS 2003 Annual Conference, Unpaginated CD-ROM, Alaska.
Sima, S., Ahmadalipour, A., Tajrishy, M., 2013. Mapping surface temperature in a hyper-saline lake and investigating the effect of temperature distribution on the lake evaporation. Remote Sens. Environ. 136, 374–385.
Song, X., Duan, Z., Jiang, X., 2012. Comparison of artificial neural networks and support vector machine classifiers for land cover classification in Northern China using a SPOT-5 HRG image. Int. J. Remote Sens. 33, 3301–3320.
Srivastava, P.K., Han, D., Rico-Ramirez, M.A., Bray, M., Islam, T., 2012. Selection of classification techniques for land use/land cover change investigation. Adv. Space Res. 50, 1250–1265.
Sun, F., Sun, W., Chen, J., Gong, P., 2012. Comparison and improvement of methods for identifying waterbodies in remotely sensed imagery. Int. J. Remote Sens. 33, 6854–6875.
Tang, Z., Ou, W., Dai, Y., Xin, Y., 2013. Extraction of water body based on LandSat TM5 imagery – a case study in the Yangtze River. Adv. Inf. Commun. Technol. 393, 416–420.
Xu, H., 2006. Modification of normalised difference water index (NDWI) to enhance open water features in remotely sensed imagery. Int. J. Remote Sens. 27, 3025–3033.
Xu, Y.B., Lai, X.J., Zhou, C.G., 2010. Water surface change detection and analysis of bottomland submersion-emersion of wetlands in Poyang Lake Reserve using ENVISAT ASAR data. Zhongguo Huanjing Kexue/China Environ. Sci. 30, 57–63.
Yocky, D.A., 1995. Image merging and data fusion by means of the discrete two-dimensional wavelet transform. J. Opt. Soc. Am. 12, 1834–1841.
Zeng, Y., Zhang, J., van Genderen, J.L., Zhang, Y., 2010. Image fusion for land cover change detection. Int. J. Image Data Fusion 1, 193–215.
Zhang, Y., 2002a. Automatic image fusion: a new sharpening technique for IKONOS multispectral images. GIM Int. 16, 54–57.
Zhang, Y., 2002b. A new automatic approach for effectively fusing Landsat 7 as well as IKONOS images. In: International Geoscience and Remote Sensing Symposium (IGARSS), pp. 2429–2431.
Zhang, Z., Prinet, V., Ma, S., 2003. Water body extraction from multi-source satellite images. Proc. IEEE Int. Geosci. Rem. Sens. Symp. 6, 3970–3972.
Zhang, Z., Lu, H., Zhao, M., Zhao, L., Zhen, H., 2009. Water body extraction and change detection based on multi-temporal SAR images. Proc. Remote Sens. GIS Data Process. Other Appl. 7498, 1–7.
Zhou, W., Wu, B., 2008. Assessment of soil erosion and sediment delivery ratio using remote sensing and GIS: a case study of upstream Chaobaihe River catchment, north China. Int. J. Sediment Res. 23, 167–173.